ANTIOXIDANTS & REDOX SIGNALING
Volume 21, Number 15, 2014

DOI: 10.1089/ars.2013.5655

Discoveries

ORIGINAL RESEARCH COMMUNICATION

RORα Decreases Oxidative Stress Through the Induction of SOD2 and GPx1 Expression and Thereby Protects Against Nonalcoholic Steatohepatitis in Mice

Yong-Hyun Han, Hyeon-Ji Kim, Eun-Jin Kim, Kyu-Seo Kim, Suckchang Hong, Hyeung-Geun Park, and Mi-Ock Lee

Abstract

Aims: Increased hepatic oxidative stress and inflammation is the main cause of exacerbating nonalcoholic steatohepatitis (NASH). Retinoic acid-related orphan receptor α (RORα) regulates diverse target genes associated with lipid metabolism, and its expression level is low in the liver of patients with NASH. Here, we investigated the role of RORα in regulating hepatic oxidative stress and inflammation. ***Results:*** First, cholesterol sulfate (CS), an agonist of RORα, lowered oxidative stress that was induced by 1.5 m*M* oleic acid in the primary cultures of hepatocytes. Second, exogenously introduced RORα or CS treatment induced the mRNA level of antioxidant enzymes, superoxide dismutase 2 (SOD2) and glutathione peroxidase 1 (GPx1), through the RORα response elements located in the upstream promoters of *Sod2* and *Gpx1*. Third, RORα significantly decreased reactive oxygen species levels and mRNA levels of tumor necrosis factor α (TNFα) and interleukin-1β that were induced by lipopolysaccharide or TNFα in Kupffer cells. Finally, the administration of JC1-40 decreased the signs of liver injury, lipid peroxidation, and inflammation in the MCD diet-induced NASH mice. ***Innovation and Conclusion:*** We showed for the first time that RORα and its ligands protect NASH in mice by reducing hepatic oxidative stress and inflammation. Further, the molecular mechanism of the protective function of RORα against oxidative stress in the liver was revealed. These findings may offer a rationale for developing therapeutic strategies against NASH using RORα ligands. *Antioxid. Redox Signal.* 21, 2083–2094.

Introduction

NONALCOHOLIC FATTY LIVER DISEASE is becoming more common worldwide, possibly because of the increasing incidence of human obesity (24). Nonalcoholic steatohepatitis (NASH) is closely associated with the metabolic complications as a result of overnutrition, including obesity and insulin resistance (22). Simple steatosis can be reversed without specific therapy; however, in some cases, it progresses to NASH, which involves fibrosis and inflammation and can progress further to cirrhosis. Indeed, NASH ranks as one of the major causes of cirrhosis, behind hepatitis C and alcoholic liver disease (3). A two-hit model has been proposed in the pathogenesis of NASH (8). The first insult is hepatic steatosis that is associated with the accumulation of lipid droplets containing triglycerides in the liver arising from an imbalance between lipid synthesis and export in hepatocytes. The second hit consists of oxidative stress, inflammation, cell death, and fibrosis. In particular, increased oxidative stress and chronic inflammation are key features of NASH, which distinguish steatohepatitis from simple steatosis (9, 19). Kupffer cells are resident macrophages that regulate liver immunity and inflammation on exposure to reactive oxygen species (ROS) (42). Increased ROS induce the activation of inflammatory transcription factor nuclear factor-kappa B (NF-κB) and enhance the production of proinflammatory cytokines such as tumor necrosis factor α (TNFα) in macrophages (10).

Retinoic acid-related orphan receptor α (RORα; NR1F1) belongs to the nuclear hormone receptor superfamily that regulates diverse target genes associated with metabolic homeostasis (13). RORα binds to ROR response elements (ROREs) in the promoter of target genes as a monomer on the monomeric half-site core 5′-AGGTCA-3′ motif or as a

Bio-MAX Institute, Research Institute of Pharmaceutical Sciences, College of Pharmacy, Seoul National University, Seoul, Korea.

Innovation

We showed for the first time that retinoic acid-related orphan receptor α (RORα) and its ligands decreased intracellular reactive oxygen species level, lipid peroxidation, and expression of inflammatory cytokines, eventually leading to attenuation of nonalcoholic steatohepatitis (NASH). RORα increased mRNA levels of superoxide dismutase 2 (SOD2) and glutathione peroxidase 1 (GPx1) in the primary hepatocytes and Kupffer cells through activation of the ROR response elements in the promoters, providing the mechanism for how RORα can protect against oxidative stress. Further, the administration of a synthetic ligand, JC1-40, confirmed the protective role of RORα in an MCD diet-induced NASH model in mice. These findings may offer a rationale for developing therapeutic strategies against NASH using RORα ligands.

homodimer on Rev-DR2 sites of direct repeats with the half site separated by 2 bps. Cholesterol derivatives, including cholesterol sulfate (CS), act as endogenous ligands that fit in the ligand-binding pocket of RORα (14, 15). RORα has been implicated in the regulation of diverse lipid and cholesterol metabolic pathways in both experimental animals and human patients. Staggerer mice ($RORα^{sg/sg}$), displaying C-terminal deletions and dysfunction of RORα, show changed metabolic homeostasis through alterations in the expression of a number of genes, such as those encoding lipin-2, acetyl-CoA carboxylase, and peroxisome proliferator-activated receptor (PPAR)γ (16). Recently, we demonstrated that RORα has dual functions, in that it activates AMP-activated protein kinase (AMPK) and represses liver X receptor α (LXRα), thereby effectively suppressing hepatic lipid accumulation (18). Several thiourea derivatives, including JC1-40, were demonstrated as activating ligands of RORα that induced activation of AMPK (28). Importantly, the administration of JC1-40 in mice dramatically attenuated hepatic steatosis (18). Further, an observation that hepatic expression level of RORα is significantly decreased when liver injury progresses to steatosis and steatohepatitis in human patients suggests that RORα may have a protective function against progression to NASH (27).

Earlier studies suggested that RORα has a protective function against oxidative stress. RORα activated the expression of antioxidant enzymes such as glutathione peroxidase 1 (GPx1) and peroxiredoxin 6 in cultured mouse neurons, thereby exhibiting a neuroprotective effect against oxidative stress that was mediated by β-amyloid, C_2-ceramide, or hydrogen peroxide (H_2O_2) (2). The treatment of melatonin, a putative ligand of RORα, reduced the level of oxidative damage and indications of neurodegeneration with increased RORα levels in the brain of mice (5, 17, 38). Although these studies suggested a potential protective role of RORα in NASH, its function in regulating oxidative stress and inflammation in fatty liver diseases has not been studied. Here, we report that RORα suppressed oxidative stress by the induction of the antioxidant enzymes, superoxide dismutase 2 (SOD2) and GPx1, and decreased the expression of proinflammatory cytokines in the liver. Further, the thiourea derivative JC1-40 significantly ameliorated hepatic injury induced by a methionine/choline-deficient (MCD) diet in mice, further supporting the role of RORα in the control of oxidative stress under conditions of an oversupply of fatty acids. This offers a rationale for developing therapeutic strategies against NASH using RORα ligands.

Results

Activation of RORα lowers intracellular ROS level and lipid peroxidation in hepatocytes

Since oxidative stress is one of the main causes of NASH, we first tested whether RORα would affect intracellular ROS level in the primary cultures of hepatocytes obtained from male Sprague–Dawley (SD) rats. To induce metabolic oxidative stress, we employed long-chain free fatty acids such as oleic acid (OA), stearic acid, and palmitic acid, which increase mitochondrial ROS generation and subsequent mitochondrial dysfunction (21, 43). The extent of intracellular ROS formation was assayed by fluorescence spectrometry of 2′,7′-dichlorodihydrofluorescein (DCF) after the incubation of cells with H_2DCF-diacetate (H_2DCFDA) and stimulation with long-chain fatty acids. Since H_2DCFDA is a probe that localizes cytosolically, increased fluorescence may represent the level of ROS derived from damaged mitochondria by increased superoxide after exposure to fatty acids (25). Treatment with 1.5 m*M* OA increased the ROS-induced fluorescence emission; however, it was decreased to basal level by cotreatment with 20 μ*M* CS, an activator of RORα (Fig. 1A). We observed similar results when hepatocytes were treated with stearic acid or palmitic acid (Supplementary Fig. S1A; Supplementary Data are available online at www.liebertpub.com/ars). The anti-oxidative function of CS was comparable with a known anti-oxidant, epigallocatechin gallate (EGCG) (Supplementary Fig. S1B) (29). The level of antioxidant cofactor glutathione (GSH) was decreased after free fatty acid treatment, but it was restored to the control level by overexpression of RORα (Supplementary Fig. S1C). When the expression of RORα was silenced by RNA interference, CS did not decrease the OA-induced ROS level, indicating that the protective effect of CS against oxidative stress was RORα dependent (Fig. 1B and Supplementary Fig. S2).

RORα enhances the transcriptional expression of SOD2 and GPx1

Intracellular ROS is efficiently scavenged by the catalytic function of antioxidant enzymes such as SOD, GPx, thioredoxin, peroxiredoxin, and catalase, and the ubiquitously present antioxidant GSH (19, 23). To elucidate the molecular mechanism of the anti-oxidative function of RORα, we examined whether expression levels of these enzymes were altered after the activation of RORα. Among these antioxidant enzymes, we found that mRNA levels of SOD2 and GPx1 were significantly elevated by CS treatment (Fig. 2 and Supplementary Fig. S3). SOD2, also called manganese superoxide dismutase, is considered one of the most important antioxidant enzymes that scavenge superoxide directly in the mitochondrial matrix (23). GPx1 is a selenocysteine-containing antioxidant enzyme that catalyzes H_2O_2—the product of SOD2 action—to H_2O (23). The treatment of CS increased the protein level of RORα as previously observed (17, 18). Similarly, protein levels of SOD2 and GPx1 were increased by CS at less than 1 μ*M* (Fig. 2A). The transduction of adenovirus (Ad)-RORα also induced the expression of SOD2 and GPx1 (Fig. 2A). The enzymatic activity of SOD2 was

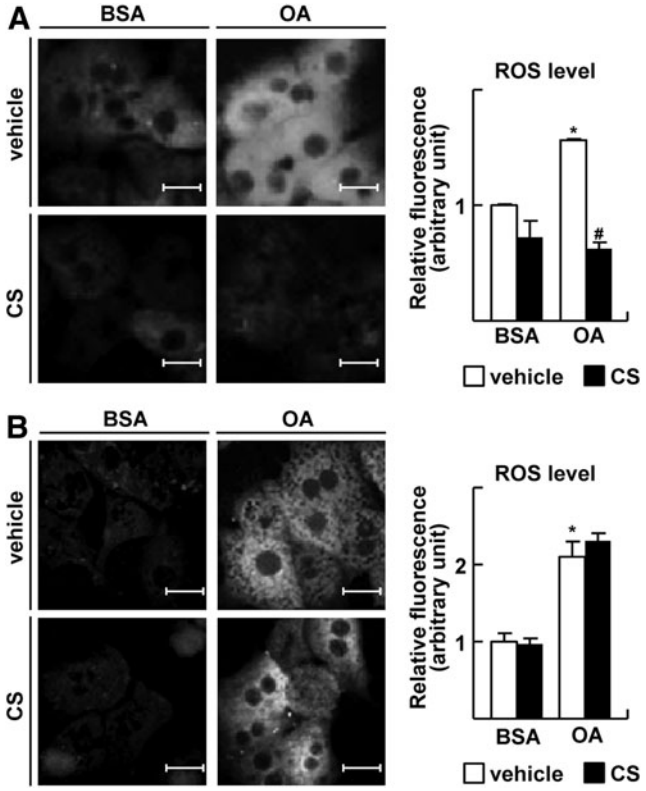

FIG. 1. RORα lowers intracellular ROS level. (A) Primary cultures of rat hepatocytes were treated with 1.5 m*M* OA and/or 20 μM CS for 24 h as indicated. **(B)** Otherwise, hepatocytes were transfected with si-RORα for 24 h, and treated with 1.5 m*M* OA and/or 20 μM CS for 24 h. At the end of treatment, cells were stained with 20 μM H_2DCFDA and visualized by fluorescence microscopy (*left*). The fluorescence intensity was quantified (*right*). BSA represents 1% BSA supplement alone as control. White bars represent 20 μm. The data represent mean ± standard deviation of three independent experiments. $^{*}p < 0.05$ *versus* BSA with vehicle; $^{\#}p < 0.05$ *versus* OA with vehicle. BSA, bovine serum albumin; CS, cholesterol sulfate; H_2DCFDA, H_2 2′,7′-dichlorodihydrofluorescein-diacetate; OA, oleic acid; RORα, retinoic acid-related orphan receptor α; ROS, reactive oxygen species.

increased after either CS treatment or Ad-mediated expression of RORα (Fig. 2B). The treatment of free fatty acids repressed GPx activity, whereas it was restored by the infection of Ad-RORα (Fig. 2B). The CS treatment did not reduce the OA-induced ROS level when SOD2 and GPx1 were silenced, confirming the involvement of these enzymes in the protective function of RORα against oxidative stress (Fig. 2C). In addition, the CS-mediated inductions of SOD2 and GPx1 protein were abolished when RORα was knocked down, indicating that the CS effect was mediated by RORα (Fig. 2D).

mRNA levels of SOD2 and GPx1 were largely increased after treatment of CS or infection of Ad-RORα, suggesting that expression of these enzymes was controlled by RORα at the transcription level (Fig. 2E). To further characterize the transcriptional induction, promoters of the human *Sod2* and the human *Gpx1* were analyzed (41). The activities of reporter encoding the *Sod2* promoter (−3318 to +104 bp) or the *Gpx1* promoter (−3460 to +618 bp) were significantly induced after CS treatment or overexpression of RORα, which were similar to that obtained after EGCG treatment (Supplementary Fig. S4). We identified putative RORα binding sites located in the 5′-upstream promoters by *in silico* analysis (6). Deletion mapping studies showed that losing the first and the second ROREs in the 5′-upstream of *Sod2* promoter and the first RORE in the 5′-upstream of *Gpx1* promoter abolished the responsiveness to RORα (Fig. 2F). Indeed, chromatin immunoprecipitation (ChIP) analysis revealed that RORα and coactivator p300 bound to the RORE2 and the RORE1 in the *Sod2* promoter and *Gpx1* promoter, respectively, in the presence of CS, indicating that these ROREs were functional to induce transcriptional activation of the genes (Fig. 2G).

Activation of RORα lowers intracellular ROS level and expression of proinflammatory cytokines in Kupffer cells

Activated Kupffer cells play an essential role in the progression of NASH by contributing to an increased production of proinflammatory cytokines and hepatic injury (9, 42). We observed that the treatment of lipopolysaccharide (LPS) or TNFα increased ROS level in the primary Kupffer cells (Fig. 3A). Similar to the observation obtained from the primary hepatocytes, the LPS- or TNFα-induced ROS levels were largely diminished by treatment with CS (Fig. 3A). Treatment with CS or infection of Ad-RORα increased mRNA levels of SOD2 and GPx1 in the Kupffer cells (Fig. 3B, C). The changes of SOD2 level was also confirmed at the protein level using immunofluorescence staining (Fig. 3D). Consistently, the infection of Ad-RORα significantly suppressed the expression of TNFα-induced proinflammatory cytokines such as TNFα itself and interleukin (IL)-1β in Kupffer cells, suggesting that suppression of ROS level by RORα may cause a decrease in the expression level of these cytokines (Fig. 3E). The activation of NF-κB induced by TNFα was largely decreased by pretreatment with CS or overexpression of RORα in RAW 264.7 (Fig. 3F). This result suggests that RORα-induced inhibition of the inflammatory responses is also associated with the disturbance of NF-κB signaling pathway in the Kupffer cells.

A synthetic RORα ligand, JC1-40, protects against progression of NASH in the MCD-diet mouse model

Previously, we reported that a synthetic thiourea compound JC1-40 activates the transcriptional function of RORα and attenuates hepatic steatosis *via* activation AMPK and inhibition of LXRα (18, 28). Here, we further demonstrated a direct binding of JC1-40 to RORα using surface plasmon resonance (SPR) technique; K_D value was evaluated as 0.9 μM from the sensorgram (Fig. 4A). Treatment with JC1-40 showed the similar effects of RORα transduction or CS treatment in that it decreased the ROS levels that were induced by OA treatment (Fig. 4B). It increased mRNA levels of Sod2 and Gpx1, which were abolished after the transfection of si-RORα (Fig. 4C). Consistently, the promoter activities of *Sod2* and *Gpx1* were increased by JC1-40 treatment (Fig. 4D). Together, these results further confirmed the protective function of RORα against oxidative stress and

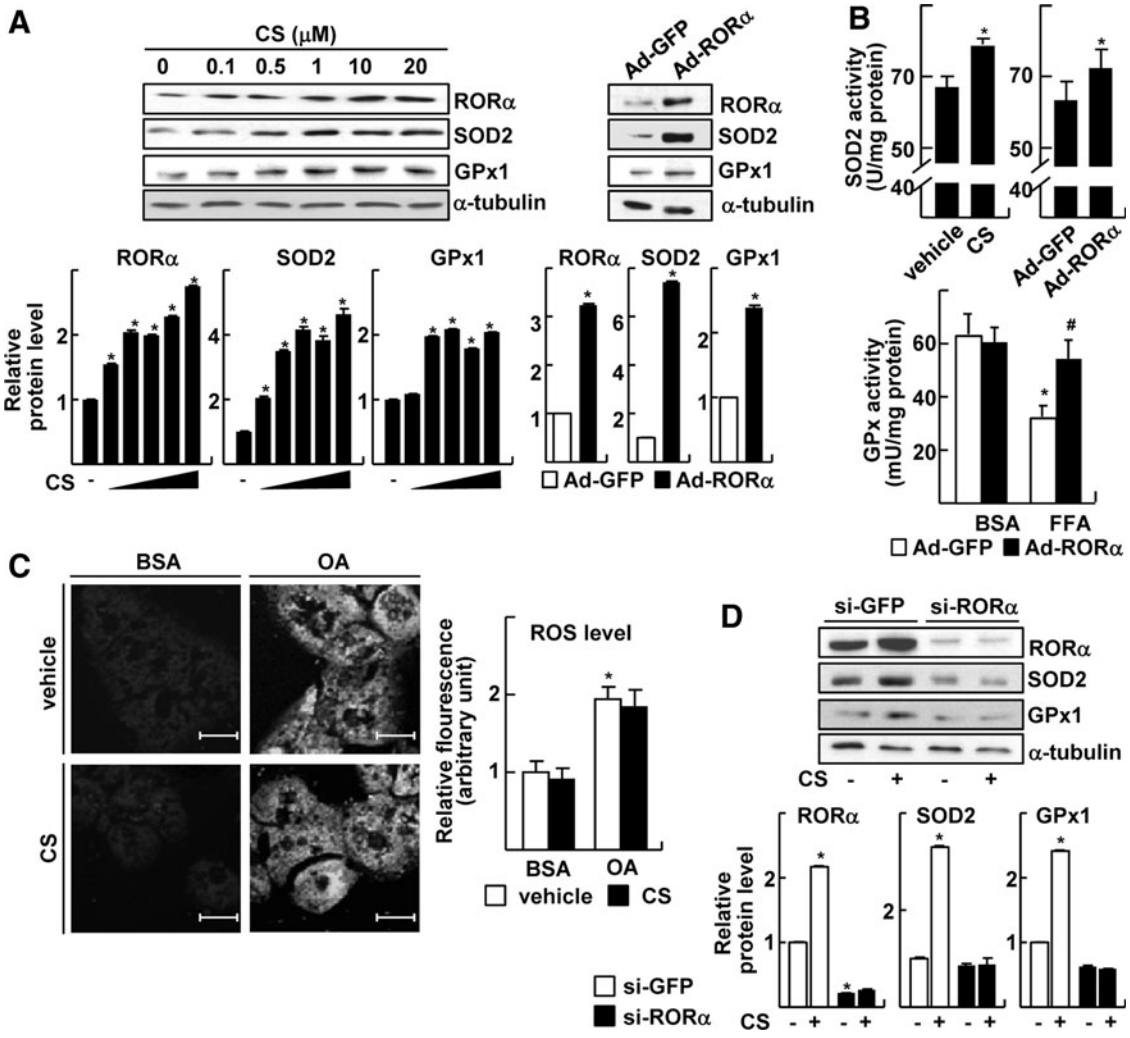

FIG. 2. RORα increases expression of SOD2 and GPx1. (A) Primary cultures of hepatocytes were treated with indicated concentrations of CS (*left*) or infected by Ad-GFP or Ad-RORα for 24 h (*right*). The expression levels of protein were measured by western blotting (*top*) and the band intensities were quantified (*bottom*). The data represent mean ± standard deviation of three independent experiments. $*p < 0.05$ *versus* vehicle treatment or Ad-GFP infection. **(B)** Hepatocytes were either treated with 20 μM CS or infected by Ads for 24 h. The enzyme activity of SOD2 in whole cell lysates was measured (*top*). Hepatocytes were infected by Ad-GFP or Ad-RORα, and treated with 0.5 m*M* FFA mixture. The enzyme activity of GPx in whole cell lysates was analyzed (*bottom*). $*p < 0.05$ *versus* Ad-GFP or vehicle treatment; $^{\#}p < 0.05$ *versus* FFA treatment with Ad-GFP infection ($n = 3$). **(C)** Hepatocytes were transfected with si-SOD2 and si-GPx1 and treated with 1.5 m*M* OA and/or 20 μM CS for 24 h. At the end of the treatment, cells were stained with 20 μM H_2DCFDA and examined by confocal fluorescence microscopy. The fluorescence intensity was quantified. BSA represents 1% BSA supplement alone as a control. The data represent mean ± standard deviation of three independent experiments. $*p < 0.05$ *versus* BSA with vehicle. **(D)** Hepatocytes were transfected with si-RORα and then treated with 20 μM CS for 24 h. The expression levels of protein were measured by western blotting (*top*), and the band intensities were quantified (*bottom*). The data represent mean ± standard deviation of three independent experiments. $*p < 0.05$ *versus* si-GFP with vehicle treatment. **(E)** Hepatocytes were treated with indicated concentrations of CS (*left*) or infected by Ad-GFP or Ad-RORα for 24 h (*right*). The mRNA levels were measured by qRT-PCR. The data represent mean ± standard deviation of three independent experiments. $*p < 0.05$ *versus* vehicle or Ad-GFP. **(F)** Schematic representation of the human *Sod2* promoter and the human *Gpx1* promoter with the putative RORα response elements shown as red boxes (*left*). HepG2 cells were transfected with the deleted *Sod2* or *Gpx1* promoter-Luc reporters with EV or p3XFLAG7.1-RORα (*right*). The data represent mean ± standard deviation of three independent experiments. $*p < 0.05$ *versus* EV. **(G)** Schematic representation for ChIP assay (*left* and *top*). HepG2 cells were treated with 20 μM CS for 24 h. DNA fragments that contain flanking region of the ROREs on the *Sod2* or *Gpx1* promoter were immunoprecipitated with the anti-RORα or anti-p300 antibodies and then amplified by PCR (*left* and *bottom*), and the band intensities were quantified (*right*). The data represent mean ± standard deviation of three independent experiments. $*p < 0.05$ *versus* vehicle treatment. EV, empty vector; Ad, adenovirus; ChIP, chromatin immunoprecipitation; GFP, green fluorescence protein; GPx1, glutathione peroxidase 1; qRT-PCR, quantitative real-time polymerase chain reaction; ROREs, ROR response elements; SOD2, superoxide dismutase 2.

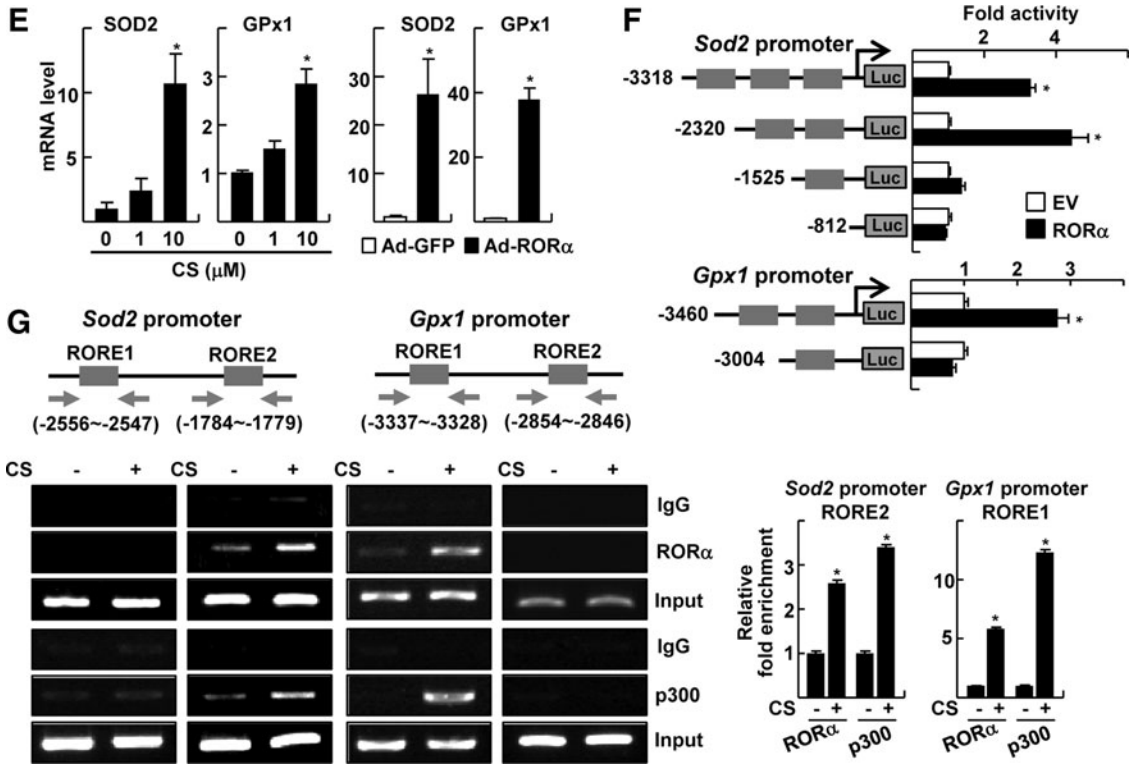

FIG. 2. (Continued).

proposed a potential therapeutic application of the compound targeting NASH.

Therefore, finally, we examined the effect of JC1-40 in the progression of NASH *in vivo* using the MCD-diet mouse model. First of all, the levels of indicators of hepatic injury—serum glutamic pyruvic transaminase (GPT) and glutamic oxaloacetate transaminase (GOT)—were significantly decreased after JC1-40 treatment (Supplementary Fig. S5A). The administration of JC1-40 for 3 weeks dramatically reduced the size and number of droplets that formed in the MCD diet fed liver (Fig. 5A). Consistently, hepatic triglyceride levels were significantly decreased after the administration of JC1-40 (Fig. 5B). The markers of lipid peroxidation, malondialdehyde (MDA) and 4-hydroxynonenal (4-HNE), markedly decreased by JC1-40 treatment when examined by ELISA and immunohistochemistry, respectively, indicating that hepatic lipid peroxidation was prevented by JC1-40 (Fig. 5B, C). Similar to the results obtained *in vitro*, the hepatic levels of mRNA as well as proteins for SOD2, GPx1, and RORα were increased in JC1-40-treated mice in both the MCD- and the methionine-choline sufficient (MCS)-diet-fed control groups (Fig. 5D, E). The data obtained from the periodic acid-Schiff with diastase (PAS-D) staining and the immunohistochemistry of the macrophage-specific marker F4/80 showed that the administration of JC1-40 largely lowered the number of total macrophages in the liver (Fig. 6A, B). Consistently, the hepatic mRNA and protein levels of F4/80, TNFα, and IL-1β were significantly decreased after the administration of JC1-40 in the MCD-diet fed mice (Fig. 6C and Supplementary Fig. S6).

Discussion

Oxidative stress generated by mitochondrial dysfunction is a critical cause of liver injury in the ''two-hits'' scenario of NASH (8). Oversupply of nutrients might induce the excessive production of mitochondrial superoxide that can be effectively converted into H_2O_2 by SOD2. Indeed, nonpeptidyl mimics of SOD2 decreased the generation of superoxide and inhibited lipid peroxidation, thereby exhibiting beneficial effects against NASH (20). However, transgenic mice overexpressing SOD2 showed enhanced susceptibility to the MCD-induced NASH when mitochondrial GSH was depleted, underscoring a key role of H_2O_2 scavenging by GPx in protecting against NASH (35). Here, we showed that RORα decreased the ROS level by increasing the activities of ROS-scavenging enzymes such as SOD2 and GPx1 (Figs. 1 and 2). The expression levels of RORα and SOD2 are significantly decreased in the livers of NASH patients and the hepatic levels of RORα and GPx1 are positively correlated in these patients, supporting a significance of our findings in human (Supplementary Fig. S7) (1). Previously, we showed that RORα induces activation of AMPK, which increases fatty acid β-oxidation and represses hepatic lipogenesis (18). Intriguingly, activation of AMPK also induces expression of multiple anti-oxidant enzymes, including SOD2, GPx, and peroxiredoxin *via* multiple mechanisms (40). However, when expression of AMPK was knocked down by transfection of si-AMPK, the degree of CS- or JC1-40-induced expression of SOD2 and GPx1 was not affected, indicating that the anti-oxidative function of RORα is mainly AMPK independent but rather dependent on the direct bindings on the promoters

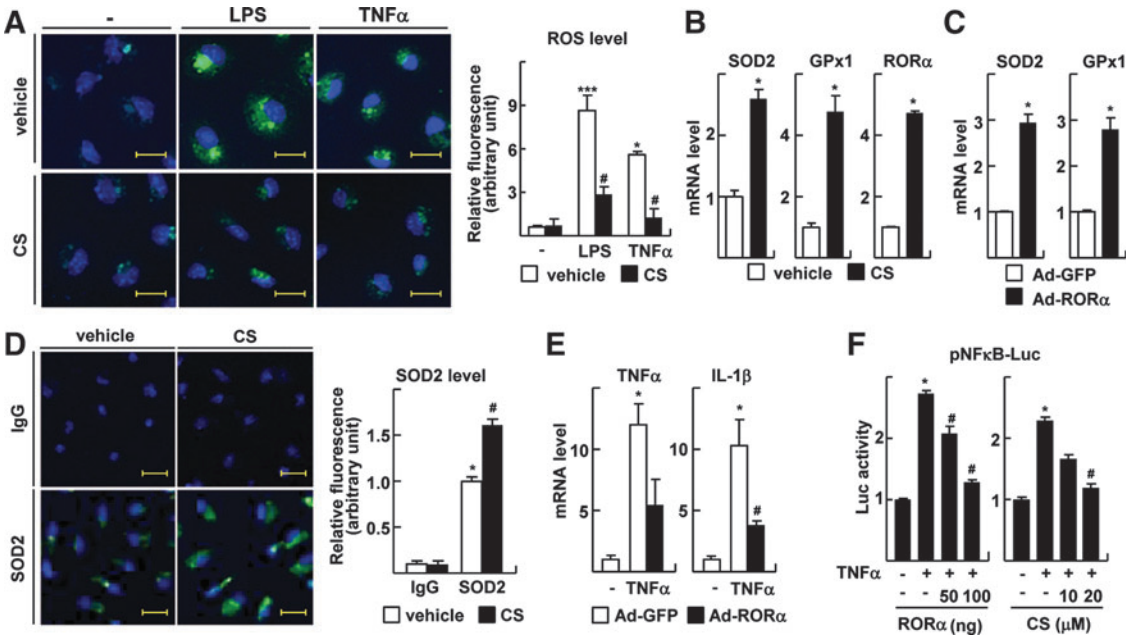

FIG. 3. RORα decreases ROS level in Kupffer cells. **(A)** Kupffer cells were treated with 10 ng/ml LPS and/or 20 μM CS for 24 h. Otherwise, Kupffer cells were treated with 20 μM CS for 18 h, and were further treated with 30 ng/ml TNFα for an additional 6 h. At the end of the treatment, cells were stained with 20 μM H_2DCFDA and examined by confocal fluorescence microscopy. Nuclei were stained by DAPI for control (*left*). The fluorescence intensity was quantified (*right*). Yellow bars represent 20 μm. The data represent mean ± standard deviation ($n = 3$). $^*p < 0.01$ and $^{***}p < 0.001$ *versus* vehicle alone; $^{\#}p < 0.05$ *versus* LPS alone or TNFα alone, respectively **(B, C)** Kupffer cells were treated with 20 μM CS **(B)** or infected by Ad-GFP or Ad-RORα **(C)**. The mRNA level was analyzed by qRT-PCR. The data represent mean ± standard deviation ($n = 3$). $^*p < 0.05$ *versus* vehicle or Ad-GFP. **(D)** Kupffer cells were treated with 20 μM CS. The expression of SOD2 was visualized by immunofluorescence (*left*), and the fluorescence intensity was quantified (*right*). The nuclei were stained by DAPI for control. Yellow bars represent 20 μm. $^*p < 0.05$ *versus* IgG with vehicle; $^{\#}p < 0.05$ *versus* α − SOD2 with vehicle **(E)** Kupffer cells were infected by Ad-GFP or Ad-RORα, and treated with 30 ng/ml TNFα for 6 h. The mRNA levels of cytokines were measured by qRT-PCR. The data represent mean ± standard deviation ($n = 3$). $^*p < 0.05$ *versus* Ad-GFP alone; $^{\#}p < 0.05$ *versus* Ad-GFP with TNFα. **(F)** RAW 264.7 cells were transfected with pNF-κB-Luc and were co-transfected with F-RORα. Otherwise, cells were treated with 20 μM CS for 18 h. Cells were further treated with TNFα for an additional 6 h. $^*p < 0.05$ *versus* vehicle; $^{\#}p < 0.05$ *versus* vehicle with TNFα ($n = 3$). The data represent mean ± standard deviation ($n = 3$). LPS, lipopolysaccharide; TNFα, tumor necrosis factor α.

of these genes as shown in Figure 2 (Supplementary Fig. S8). Therefore, both functions of RORα in inducing multiple antioxidant enzymes and in attenuating hepatic steatosis through activation of AMPK may effectively contribute to protection of the liver against NASH.

Kupffer cells have been implicated in the pathogenesis of various liver diseases, including viral hepatitis, steatohepatitis, and liver fibrosis (9). These cells secrete various cytokines, including TNFα and IL-1β, on exposure to LPS, adipokines, and oxidative stress, which induce hepatic inflammatory signaling in autocrine and paracrine mechanisms (42). A growing volume of evidence supports the role of Kupffer cells in hepatic lipid metabolism. Huang *et al.* and Tosello-Trampont *et al.* showed that TNFα released from Kupffer cells played an important role in inducing hepatic steatosis and insulin resistance and further determined a crucial phase in NASH development (11, 34). Kupffer cells induced hepatic triglyceride storage, at least partially, through the secretion of IL-1β, which, in turn, repressed PPARα activity (33). Further, treatment with saturated FAs activated the inflammasome, which cleaves pro-IL-1β into secreted IL-1β in hepatocytes, which amplified the inflammation loop by activating liver mononuclear cells (7). Together, these results suggest that TNFα and IL-1β produced by Kupffer cells might integrate the first ''hit'' to the second one that accelerates the progression of NASH. RORα attenuates hepatic triglyceride accumulation *via* the activation of AMPK and the suppression of LXRα and its lipogenic target genes (18). In addition, here, we demonstrated that RORα repressed the production of TNFα and IL-1β in Kupffer cells (Fig. 3), indicating that RORα might disrupt the vicious cycle of steatosis connecting to steatohepatitis.

Many researchers have endeavored to find appropriate therapeutic strategies for patients with NASH. So far, activating agonists of PPARs such as Wy-14,643 and rosiglitazone have been tested for their effectiveness in diminishing the symptoms of NASH (12, 39). However, the trials have not yet been successful, because the clinically applied PPAR agonists, rosiglitazone and pioglitazone, have several side effects such as edema, increased adiposity, liver toxicity, myocardial infarction, and heart failure (30, 31). Recently, the identification of ligands for RORα has expanded the search for synthetic ligands (32). The synthetic ligand SR1078 that is a specific RORα/γ agonist was identified through modifying an analog of TO901317, an inverse agonist of RORα with a relatively wide spectrum of specificity

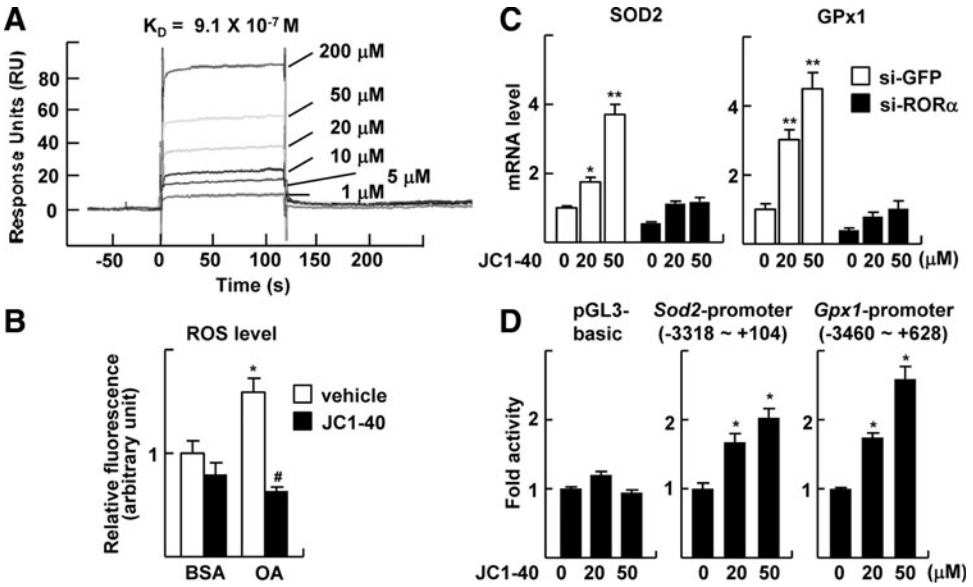

FIG. 4. A thiourea derivative JC1-40 protects oxidative stress through induction of SOD2 and GPx1. (A) BIAcore analysis for binding of JC1-40 to RORα. The increasing concentrations of JC1-40 were injected over immobilized GST-RORα-His proteins on the sensor chip. **(B)** Hepatocytes were treated with 1.5 m*M* OA and/or 20 μM JC1-40 for 24 h. At the end of the treatment, cells were stained with 20 μM H_2DCFDA and visualized by fluorescence microscopy. The fluorescence intensity was quantified. BSA represents 1% BSA supplement alone as a control. The data represent mean ± standard deviation of three independent experiments. $^*p < 0.05$ *versus* BSA with vehicle; $^{\#}p < 0.05$ *versus* OA with vehicle. **(C)** HepG2 cells were transfected with si-GFP or si-RORα and then treated with the indicated concentrations of JC1-40 for 24 h. The expression levels of mRNA were measured by qRT-PCR. The data represent mean ± standard deviation ($n = 3$). $^*p < 0.05$ and $^{**}p < 0.01$ *versus* si-GFP with vehicle. **(D)** HepG2 cells were transfected with the pGL3 basic-Luc, the *Sod2* promoter-Luc, or the *Gpx1* promoter-Luc reporter and treated with JC1-40 for 24 h. The data represent mean ± standard deviation ($n = 3$). $^*p < 0.05$ *versus* vehicle. GST, glutathione *S*-transferase.

(36). However, its function in regulating physiological metabolisms remains elusive. Here, we demonstrated that JC1-40 directly binds the ligand-binding domain of RORα (Fig. 4A), which indicates JC1-40 to be an activating agonist of RORα. Based on our findings, JC1-40 decreased the free fatty acid-induced intracellular ROS levels in the hepatocytes, extent of lipid peroxidation, and production of proinflammatory cytokines in a mouse model of NASH (Fig. 6D). In addition, when liver sections obtained from the MCD-diet-fed mice were examined for collagen deposition by Sirius red staining, JC1-40 treatment dramatically reduced collagenous fibrosis. Consistently, the transcription levels of pro col1a1, a precursor of collagen type I, and transforming growth factor β (TGFβ), a fibrogenic mediator secreted from Kupffer cells, were significantly lowered by JC1-40 in the liver of MCD diet-fed mice (Supplementary Fig. S9). Together, these results further suggest that JC1-40 could contribute to developing clinically suitable RORα agonists which could be useful in preventing and curing NASH.

Materials and Methods

Cell culture and reagents

Hepatocytes and Kupffer cells were isolated from 7- to 10 week-old, male SD rats (Charles River Laboratories, Wilmington, MA) by perfusion of the liver using collagenase type IV (Sigma-Aldrich, St Louis, MO) (9). The cell pellet containing hepatocytes was plated onto collagen-coated plates with Williams Medium (Invitrogen, Carlsbad, CA) that was supplemented with 10% fetal bovine serum (FBS), 0.01% insulin, and 0.004% dexamethasone. For the isolation of Kupffer cells, nonparenchymal sufficient supernatant was centrifuged in 50%/25% percoll (GE Healthcare, Waukesha, WI). The layer containing Kupffer cells was plated with RPMI 1640 (Hyclone, Logan, UT) with 10% FBS. The purity of Kupffer cells exceeded 85% when estimated by immunocytochemistry using CD68 antibody (Serotec, Oxford, United Kingdom). HepG2 and RAW 264.7 were obtained from American Type Culture Collection (ATCC, Rockville, MD) and cultured in Dulbecco's modified Eagle's medium (Hyclone) that was supplemented with 10% FBS. The cells were grown in an incubator with 5% CO_2 and 95% air at 37°C.

CS, an activator of RORα, and OA, a mono-unsaturated fatty acid, with 98% and 99% purities, respectively, were purchased from Sigma-Aldrich. The synthesis and preparation of JC1-40, an agonistic ligand of RORα, were previously reported (18, 28).

Plasmids, si-RNA, recombinant Ad, and transient transfection

The human *Sod2* promoter reporters were either kindly provided by Dr. Yong Xu (University of Kentucky, Lexington, KY) or constructed by conventional recombinant procedures (41). The *Gpx1* promoters encoding regions of −3460 to +628 and −3004 to +628, relative to the transcription start site, were amplified by PCR and cloned into *Bgl*II/*Hind*III site of the pGL3-basic vector. FLAG-tagged RORα, and the recombinant Ads encoding RORα or green

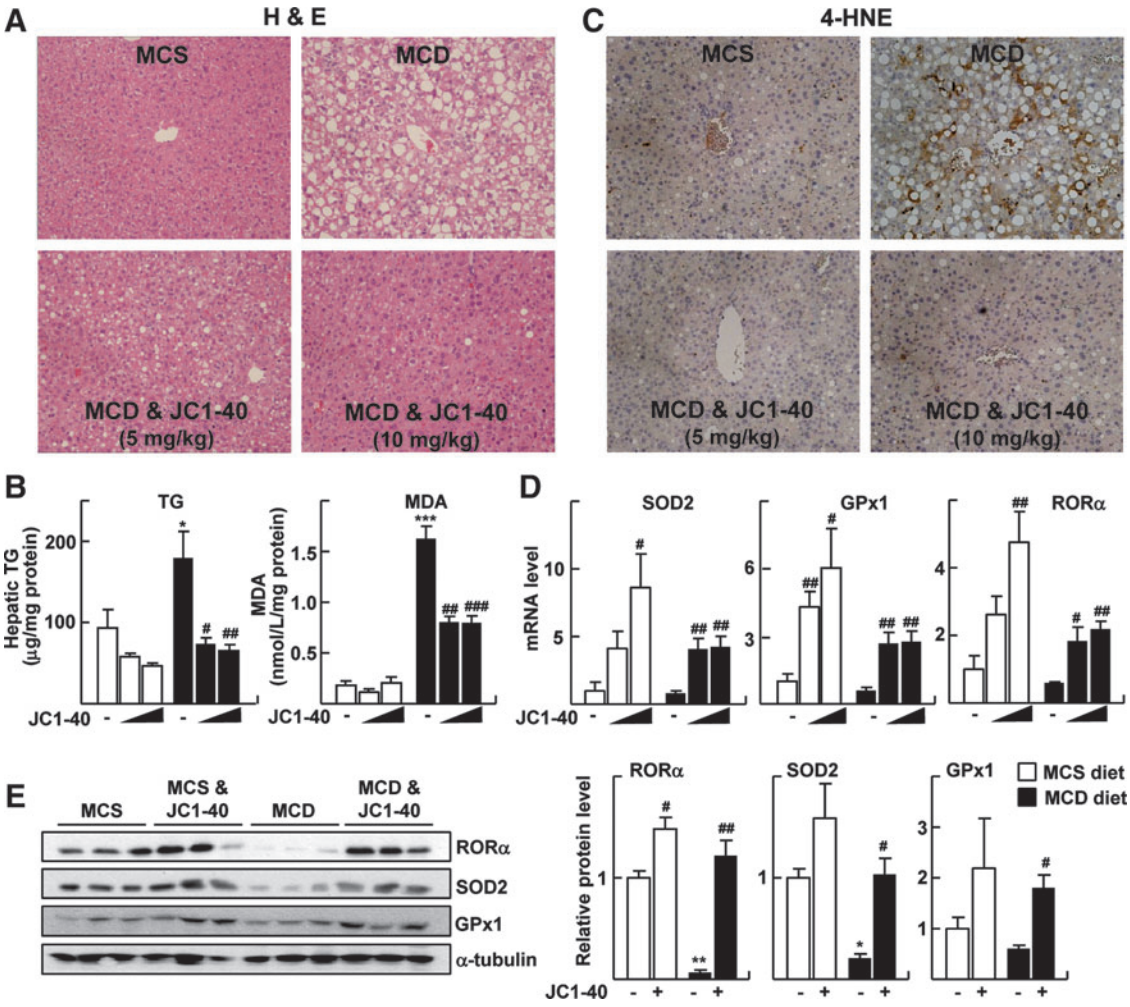

FIG. 5. Administration of JC1-40 attenuates the MCD diet-induced NASH. Eight-week-old C57BL/6N mice were fed with either MCS or MCD diet for 4 weeks. After 1 week of diet feeding, JC1-40 was administered daily at doses of 5 and 10 mg/kg/day by oral gavage. **(A)** H&E staining of liver sections. Magnification of ×200. **(B)** Amounts of TG and MDA in the liver were analyzed. The data represent mean ± standard deviation. $*p<0.05$ and $***p<0.001$ *versus* MCS diet with vehicle ($n=4$); $^{\#}p<0.05$, $^{\#\#}p<0.01$, and $^{\#\#\#}p<0.001$ *versus* MCD diet with vehicle ($n=5$). **(C)** Immunohistochemistry staining of 4-HNE in liver sections. Magnification of ×200. **(D)** mRNA expression levels of SOD2, GPx1, and RORα were analyzed by qRT-PCR. The data represent mean ± standard deviation. $^{\#}p<0.05$ and $^{\#\#}p<0.01$ *versus* MCS diet with vehicle ($n=4$) or MCD diet with vehicle ($n=5$). **(E)** Protein expression levels of SOD2, GPx1, and RORα were analyzed by western blotting (*left*), and the band intensities were quantified (*right*). The data represent mean ± standard deviation. $*p<0.05$ and $**p<0.01$ *versus* MCS diet with vehicle; $^{\#}p<0.05$ and $^{\#\#}p<0.01$ *versus* MCD diet with vehicle. TG, triglycerides; 4-HNE, 4-hydroxynonenal; H&E, hematoxylin and eosin; MCS, methionine-choline sufficient; MDA, malondialdehyde; NASH, nonalcoholic steatohepatitis.

fluorescence protein (GFP), that is, Ad-RORα or Ad-GFP, were previously described (17, 18). The small interference RNA (si-RNA) duplex targeting rat RORα (5′-UACGUGU GAAGGCUGCAAGGGC-3′) and control nonspecific si-RNA were synthesized from Shamchully Pharm, Co., Ltd (Seoul, Korea). The si-RNA targeting rats SOD2 and GPx1 were purchased from Sigma-Aldrich. The transient transfection to the primary hepatocytes was carried out using Lipofectamine 2000 (Invitrogen).

Western blotting, immunofluorescence staining, and ChIP analysis

Western blotting was carried out as previously described using specific antibodies against RORα (Thermo Scientific, Waltham, MA), SOD2 (Milipore, Billerica, MA), GPx1 (Santa Cruz Biotechnology, Santa Cruz, MA), or α-tubulin (Calbiochem, La Jolla, CA) (18). The band intensity was quantified by image J software (http://rsb.info.nih.gov) and normalized by that of α-tubulin. Immunofluorescence staining was performed with a specific antibody against SOD2 (Milipore) and the Alexa Fluor 488-conjugated secondary antibody (Invitrogen). ChIP assay was performed as previously described using specific primers (Supplementary Table S1) (18). The band intensity was quantified by image J software and normalized by that of the input.

Quantitative real-time polymerase chain reaction

Total RNA was isolated using Easy-Blue reagents (INtRON Biotechnology, Seoul, Korea) according to the manufacturer's protocol. The concentration and purity of RNA

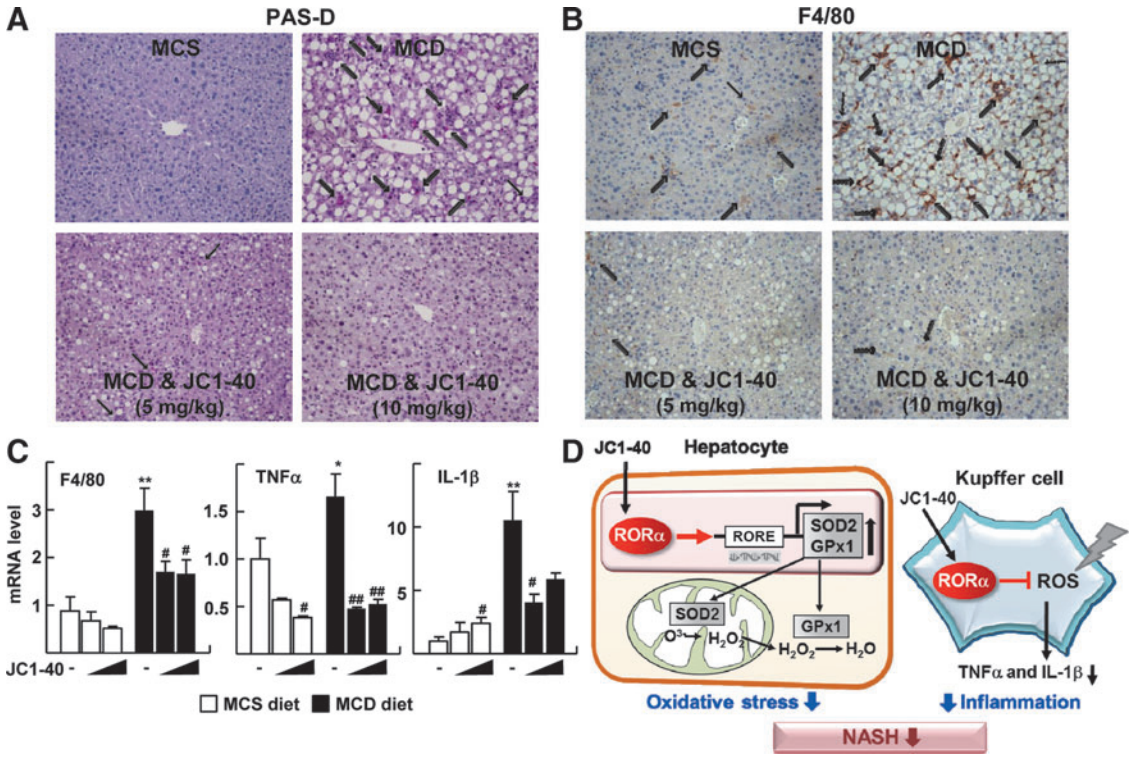

FIG. 6. JC1-40 suppresses the MCD diet-induced pro-inflammatory responses. **(A)** Liver sections were stained with PAS-D staining. Stained macrophages are indicated by *arrows*. Magnification of ×200 (*top*). **(B)** Immunohistochemistry staining of F4/80 in liver sections. Stained F4/80 positive macrophages are indicated by *arrows*. Magnification of ×200. **(C)** mRNA expression levels of cytokines were analyzed by qRT-PCR. The data represent mean ± standard deviation. $*p < 0.05$ and $**p < 0.01$ *versus* MCS diet with vehicle ($n = 4$); $^{\#}p < 0.05$ and $^{\#\#}p < 0.01$ *versus* MCS diet with vehicle ($n = 4$) or MCD diet with vehicle ($n = 5$). **(D)** Schematic model for the protective role of RORα against progression of NASH. PAS-D, periodic acid-Schiff with diastase.

were assessed in NanoDrop® ND 1000 UV-Vis Spectrophotometer (Thermo Scientific). About 1.5–2.0 μg RNA was reverse transcribed into cDNA using 0.06 ng random hexamer in the first strand buffer containing 10 m*M* dithiothreitol, 0.5 m*M* oligo dNTP, and 200 U murine myeloleukemia virus reverse transcriptase (Invitrogen). Quantitative real-time polymerase chain reaction (qRT-PCR) experiments were performed using an ABI StepOnePlus™ Real-time PCR system (Applied Biosystem, Foster City, CA). Reactions were performed in 10 μl volumes, which included 37.5–50 ng cDNA, 5 pmols of each primer, and SYBR® Green PCR Master Mix. Primer sequences are listed in Supplementary Table S2. Conditions for amplification were 95°C for 10 min, followed by 40 cycles of 95°C for 15 s, and 60°C for 1 min. Relative mRNA level of target gene was estimated by the equation $2^{-\Delta Ct}$ ($\Delta Ct = Ct$ of target gene minus Ct of β-actin). Fold inductions in the mRNA level of genes were presented with a level of the control group set as 1 (4).

Measurement of intracellular ROS level

Primary cultures of hepatocytes were seeded in a 12-well plate and grown for 18 h. After the complete medium was changed to FBS-free medium for starvation, cells were treated with 1.5 m*M* OA that was conjugated with bovine serum albumin (BSA). Stock solutions of 1.5 m*M* fatty acid were prepared in culture medium containing 1% fatty acid-free BSA, and they were conveniently diluted in culture medium to obtain the desired final concentrations. Kupffer cells were treated with 10 ng/ml LPS (Sigma-Aldrich) for 24 h or 30 ng/ml TNFα (Sigma-Aldrich) for 6 h. Intracellular ROS levels were estimated using H_2DCFDA (Invitrogen), an oxidation-specific fluorogenic probe that exhibits reactivity after conversion into its hydrophilic derivative $DCFH_2$ toward many oxidizing compounds. Although $DCFH_2$ has very low activity toward H_2O_2, it can facilitate oxidation indirectly *via* peroxidase-metal catalyzed reactions and heme reactions (37). At the end of the treatment, culture media was removed, cells were washed with phosphate-buffered saline (PBS), and incubated in PBS containing 20 μ*M* H_2DCFDA for 20 min at 37°C. The fluorescence of cells was examined by an LSM700 confocal microscope (excitation wavelength at 488 nm; Carl Zeiss, New York, NY). The fluorescence intensity was quantified by image J software and normalized by the number of cells in the field.

Ligand binding analysis using SPR of BIAcore

For the recombinant protein production in *Escherichia coli*, the pET21a$^+$-GST-RORα-His was transformed to B21 (DE5) cells, grown at 37°C in LB medium, and induced with 0.5 m*M* isopropyl β-D-1-thiogalactopyranoside for 6 h at 30°C. The supernatant of bacteria lysates was loaded to Ni^+-NTA resin (Qiagen, Valencia, CA) for His-tag affinity column chromatography. After a wash with the buffer containing 50 m*M* Tris-HCl (pH 8.0), 100 m*M* NaCl, and 50 m*M* imidazole, the

resin-bound glutathione *S*-transferase (GST)-RORα-His proteins were eluted by increasing the concentration of imidazole from 250 to 500 m*M*. The purified GST-RORα-His proteins were dialyzed and eluted with PBS-T buffer containing 137 m*M* NaCl, 2.7 m*M* KCl, 8.1 m*M* Na_2HPO_4, 1.8 m*M* KH_2PO_4, and 0.1% Tween 20.

SPR experiments were performed by using a BIAcore 3000 system (GE Healthcare). The GST-RORα-His proteins were immobilized onto the CM5 sensor chip (GE Healthcare). JC1-40 was dissolved in PBS-T with 0.01% DMSO, injected at a flow rate of 30 μl/min. Affinity constants (K_D) were derived using the nonlinear fitting with the simple 1:1 Langmuir binding model by the BIA evaluation 3.1 software (Biacore AB, Uppsala, Sweden).

Animals, treatments, and histological analysis

All animal experiments were conducted in accordance with the guidelines of Seoul National University Institutional Animal Care and Use Committee. Male, 8-week-old C57BL/6 mice were obtained from Charles River Laboratories and housed in an air-conditioned room at a temperature of 22°C–24°C and a humidity of 37%–64%, with a 12-h light/dark cycle. Mice were fed for 4 weeks with an MCD diet or an MCS diet that served as a control (Dyets, Inc., Bethlehem, PA). The animals were fed with an iso-caloric diet, and the nutritional compositions of the MCS and MCD diets are shown in Supplementary Table S3. After 1 week of diet feeding, JC1-40, suspended in 0.5% carboxymethyl cellulose, was dosed by oral gavage with 5 and 10 mg/kg/day for 3 weeks. At the end of the experiments, mice were fasted for 12 h. After the animals were sacrificed, their livers were removed. The information on body weight and liver weight was provided as Supplementary Figure S5B. A cross-section of the left lobe of the liver was collected and fixed in 10% neutral-buffered formalin. The fixed liver tissues were dehydrated, embedded in paraffin, sectioned to 3 μm thicknesses, and processed for hematoxylin and eosin (H&E) staining or histopathological examinations. Macrophages in the liver sections were stained by either the diastase/periodic acid-Schiff method or immunohistochemistry using F4/80 antibodies. 4-HNE, a biological marker of lipid peroxidation, was stained using specific antibodies (JalCA, Shizuoka, Japan). In addition, the expression of proinflammatory cytokines, TNFα and IL-1β (Santa Cruz Biotechnology), was analyzed by immunohistochemistry, as previously described (26).

Measurement of enzyme activity of SOD2 and GPx

Primary hepatocytes were seeded in a six-well plate and incubated overnight. Cells were infected by Ad-GFP, Ad-RORα1, or treated with CS for 24 h. The activity of SOD2 was measured using the SOD assay kit (Cayman Chemical, Ann Arbor, MI). The addition of 3 m*M* potassium cyanide that inhibits Cu/Zn SOD and extracellular SOD results in the detection of only SOD2 activity. The activity of GPx was measured using the Bioxytech™ GPx-340 assay kit (Oxisresearch, Portland, Oregon).

Measurement of triglyceride, GSH, and MDA

Amounts of MDA and GSH were assessed using the Bioxytech MDA-586 assay kit and Bioxytech GSH/GSSG-412 assay kit, respectively (Oxisresearch). Triglyceride concentration was measured using the EnzyChrom™ Triglyceride Assay Kit (Bio Assay Systems, Hayward, CA).

Statistics

All values were expressed as means ± standard deviation. Statistical analysis was performed using nonparametric Mann–Whitney *U* test for simple comparisons or Kruskal–Wallis ANOVA for multiple comparisons. $p < 0.05$ was considered statistically different.

Acknowledgments

This study was supported by grants from the NRF (2009-0080757), the SRC/ERC (R11-2007-107-01001-0), and the Bio & Medical Technology Development Program (2012M3A9B6055338).

Authors' Contributions

The corresponding author certifies that all of the listed authors participated meaningfully in the study and that they had seen and approved the final article.

Author Disclosure Statement

The authors declare that there are no conflicts of interest.

References

1. Baker SS, Baker RD, Liu W, Nowak NJ, and Zhu L. Role of alcohol metabolism in non-alcoholic steatohepatitis. *PLoS One* 5: e9570, 2010.
2. Boukhtouche F, Vodjdani G, Jarvis CI, Bakouche J, Staels B, Mallet J, Mariani J, Lemaigre-Dubreuil Y, and Brugg B. Human retinoic acid receptor-related orphan receptor alpha1 overexpression protects neurones against oxidative stress-induced apoptosis. *J Neurochem* 96: 1778–1789, 2006.
3. Bugianesi E, Leone N, Vanni E, Marchesini G, Brunello F, Carucci P, Musso A, De Paolis P, Capussotti L, Salizzoni M, and Rizzetto M. Expanding the natural history of nonalcoholic steatohepatitis: From cryptogenic cirrhosis to hepatocellular carcinoma. *Gastroenterology* 123: 134–140, 2002.
4. Bustin SA, Benes V, Garson JA, Hellemans J, Huggett J, Kubista M, Mueller R, Nolan T, Pfaffl MW, Shipley GL, Vandesompele J, and Wittwer CT. The MIQE guidelines: minimum information for publication of quantitative real-time PCR experiments. *Clin Chem* 55: 611–622, 2009.
5. Caballero B, Vega-Naredo I, Sierra V, Huidobro-Fernández C, Soria-Valles C, De Gonzalo-Calvo D, Tolivia D, Gutierrez-Cuesta J, Pallas M, Camins A, Rodríguez-Colunga MJ, and Coto-Montes A. Favorable effects of a prolonged treatment with melatonin on the level of oxidative damage and neurodegeneration in senescence-accelerated mice. *J Pineal Res* 45: 302–311, 2008.
6. Cartharius K, Frech K, Grote K, Klocke B, Haltmeier M, Klingenhoff A, Frisch M, Bayerlein M, and Werner T. MatInspector and beyond: promoter analysis based on transcription factor binding sites. *Bioinformatics* 21: 2933–2942, 2005.
7. Csak T, Ganz M, Pespisa J, Kodys K, Dolganiuc A, and Szabo G. Fatty acid and endotoxin activate inflammasomes

in mouse hepatocytes that release danger signals to stimulate immune cells. *Hepatology* 54: 133–144, 2011.
8. Day CP and James OF. Steatohepatitis: a tale of two ''hits''? *Gastroenterology* 114: 842–845, 1998.
9. Farrell GC, van Rooyen D, Gan L, and Chitturi S. NASH is an inflammatory disorder: pathogenic, prognostic and therapeutic implications. *Gut Liver* 6: 149–171, 2012.
10. Forman HJ and Torres M. Redox signaling in macrophages. *Mol Aspects Med* 22: 189–216, 2001.
11. Huang W, Metlakunta A, Dedousis N, Zhang P, Sipula I, Dube JJ, Scott DK, and O'Doherty RM. Depletion of liver Kupffer cells prevents the development of diet-induced hepatic steatosis and insulin resistance. *Diabetes* 59: 347–357, 2010.
12. Ip E, Farrell G, Hall P, Robertson G, and Leclercq I. Administration of the potent PPARalpha agonist, Wy-14,643, reverses nutritional fibrosis and steatohepatitis in mice. *Hepatology* 39: 1286–1296, 2004.
13. Jetten AM. Retinoid-related orphan receptors (RORs): critical roles in development, immunity, circadian rhythm, and cellular metabolism. *Nucl Recept Signal* 7: e003, 2009.
14. Kallen J, Schlaeppi JM, Bitsch F, Delhon I, and Fournier B. Crystal structure of the human RORalpha ligand binding domain in complex with cholesterol sulfate at 2.2 A. *J Biol Chem* 279: 14033–14038, 2004.
15. Kallen JA, Schlaeppi JM, Bitsch F, Geisse S, Geiser M, Delhon I, and Fournier B. X-ray structure of the hROR-alpha LBD at 1.63 A: structural and functional data that cholesterol or a cholesterol derivative is the natural ligand of RORalpha. *Structure* 10: 1697–1707, 2002.
16. Kang HS, Okamoto K, Takeda Y, Beak JY, Gerrish K, Bortner CD, DeGraff LM, Wada T, Xie W, and Jetten AM. Transcriptional profiling reveals a role for RORalpha in regulating gene expression in obesity-associated inflammation and hepatic steatosis. *Physiol Genomics* 43: 818–828, 2011.
17. Kim EJ, Yoo YG, Yang WK, Lim YS, Na TY, Lee IK, and Lee MO. Transcriptional activation of HIF-1 by RORalpha and its role in hypoxia signaling. *Arterioscler Thromb Vasc Biol* 28: 1796–1802, 2008.
18. Kim EJ, Yoon YS, Hong S, Son HY, Na TY, Lee MH, Kang HJ, Park J, Cho WJ, Kim SG, Koo SH, Park HG, and Lee MO. Retinoic acid receptor-related orphan receptor α-induced activation of adenosine monophosphate-activated protein kinase results in attenuation of hepatic steatosis. *Hepatology* 55: 1379–1388, 2012.
19. Koek GH, Liedorp PR, and Bast A. The role of oxidative stress in non-alcoholic steatohepatitis. *Clin Chim Acta* 412: 1297–1305, 2011.
20. Laurent A, Nicco C, Tran Van Nhieu J, Borderie D, Chéreau C, Conti F, Jaffray P, Soubrane O, Calmus Y, Weill B, and Batteux F. Pivotal role of superoxide anion and beneficial effect of antioxidant molecules in murine steatohepatitis. *Hepatology* 39: 1277–1285, 2004.
21. Malhi H and Gores GJ. Molecular mechanisms of lipotoxicity in nonalcoholic fatty liver disease. *Semin Liver Dis* 28: 360–369, 2008.
22. Marchesini G, Bugianesi E, Forlani G, Cerrelli F, Lenzi M, Manini R, Natale S, Vanni E, Villanova N, Melchionda N, and Rizzetto M. Nonalcoholic fatty liver, steatohepatitis, and the metabolic syndrome. *Hepatology* 37: 917–923, 2003.
23. Matés JM, Pérez-Gómez C, and Núñez de Castro I. Antioxidant enzymes and human diseases. *Clin Biochem* 32: 595–603, 1999.
24. Miyake T, Kumagi T, Hirooka M, Furukawa S, Koizumi M, Tokumoto Y, Ueda T, Yamamoto S, Abe M, Kitai K, Hiasa Y, Matsuura B, and Onji M. Body mass index is the most useful predictive factor for the onset of nonalcoholic fatty liver disease: a community-based retrospecitve longitudinal cohor study. *J Gastroenterol* 48: 413–422, 2013.
25. Murphy MP. How mitochondria produce reactive oxygen species. *Biochem J* 417: 1–13, 2009.
26. Na TY, Shin YK, Roh KJ, Kang SA, Hong I, Oh SJ, Seong JK, Park CK, Choi YL, and Lee MO. Liver X receptor mediates hepatitis B virus X protein-induced lipogenesis in hepatitis B virus-associated hepatocellular carcinoma. *Hepatology* 49: 1122–1131, 2009.
27. Ou Z, Shi X, Gilroy RK, Kirisci L, Romkes M, Lynch C, Wang H, Xu M, Jiang M, Ren S, Gramignoli R, Strom SC, Huang M, and Xie W. Regulation of the human hydroxysteroid sulfotransferase (SULT2A1) by RORα and RORγ and its potential relevance to human liver diseases. *Mol Endocrinol* 27: 106–115, 2013.
28. Park Y, Hong S, Lee M, Jung H, Cho WJ, Kim EJ, Son HY, Lee MO, and Park HG. N-methylthioureas as new agonists of retinoic acid receptor-related orphan receptor. *Arch Pharm Res* 35: 1393–1401, 2012.
29. Saha P and Das S. Elimination of deleterious effects of free radicals in murine skin carcinogenesis by black tea infusion, theaflavins and epigallocatechin gallate. *Asian Pac J Cancer Prev* 3: 225–230, 2002.
30. Singh S, Loke YK, and Furberg CD. Long-term risk of cardiovascular events with rosiglitazone: a meta-analysis. *JAMA* 298: 1189–1195, 2007.
31. Shah P and Mudaliar S. Pioglitazone: side effect and safety profile. *Expert Opin Drug Saf* 9: 347–354, 2010.
32. Solt LA and Burris TP. Action of RORs and their ligands in (patho)physiology. *Trends Endocrinol Metab* 23: 619–627, 2012.
33. Stienstra R, Saudale F, Duval C, Keshtkar S, Groener JE, van Rooijen N, Staels B, Kersten S, and Müller M. Kupffer cells promote hepatic steatosis *via* interleukin-1beta-dependent suppression of peroxisome proliferator-activated receptor alpha activity. *Hepatology* 51: 511–522, 2010.
34. Tosello-Trampont AC, Landes SG, Nguyen V, Novobrantseva TI, and Hahn YS. Kupffer cells trigger nonalcoholic steatohepatitis development in diet-induced mouse model through tumor necrosis factor-α production. *J Biol Chem* 287: 40161–40172, 2012.
35. von Montfort C, Matias N, Fernandez A, Fucho R, Conde de la Rosa L, Martinez-Chantar ML, Mato JM, Machida K, Tsukamoto H, Murphy MP, Mansouri A, Kaplowitz N, Garcia-Ruiz C, and Fernandez-Checa JC. Mitochondrial GSH determines the toxic or therapeutic potential of superoxide scavenging in steatohepatitis. *J Hepatol* 57: 852–829, 2012.
36. Wang Y, Kumar N, Nuhant P, Cameron MD, Istrate MA, Roush WR, Griffin PR, and Burris TP. Identification of SR1078, a synthetic agonist for the orphan nuclear receptors RORα and RORγ. *ACS Chem Biol* 5: 1029–1034, 2010.
37. Wardman P. Fluorescent and luminescent probes for measurement of oxidative and nitrosative species in cells and

tissues: progress, pitfalls, and prospects. *Free Radic Biol Med* 43: 995–1022, 2007.
38. Wiesenberg I, Missbach M, Kahlen JP, Schräder M, and Carlberg C. Transcriptional activation of the nuclear receptor RZR alpha by the pineal gland hormone melatonin and identification of CGP 52608 as a synthetic ligand. *Nucleic Acids Res* 23: 327–333, 1995.
39. Wu CW, Chu ES, Lam CN, Cheng AS, Lee CW, Wong VW, Sung JJ, and Yu J. PPARgamma is essential for protection against nonalcoholic steatohepatitis. *Gene Ther* 17: 790–798, 2010.
40. Wu S, Wu Y, Wu T, and Wei Y. Role of AMPK-mediated adaptive responses in human cells with mitochondrial dysfunction to oxidative stress. *Biochim Biophys Acta* 1840: 1331–1344, 2014.
41. Xu Y, Porntadavity S, and St Clair DK. Transcriptional regulation of the human manganese superoxide dismutase gene: the role of specificity protein 1 (Sp1) and activating protein-2 (AP-2). *Biochem J* 362: 401–412, 2002.
42. Zhan YT and An W. Roles of liver innate immune cells in nonalcoholic fatty liver disease. *World J Gastroenterol* 16: 4652–4660, 2010.
43. Zhang D, Xie L, Wei Y, Liu Y, Jia G, Zhou F, and Ji B. Development of a cell-based antioxidant activity assay using dietary fatty acid as oxidative stressor. *Food Chem* 141: 347–356, 2013.

Address correspondence to:
Dr. Mi-Ock Lee
Bio-MAX Institute
Research Institute of Pharmaceutical Sciences
College of Pharmacy
Seoul National University
San 56-1 Sillim-Dong
Kwanak-Gu
Seoul 151-742
Korea

E-mail: molee@snu.ac.kr

Date of first submission to ARS Central, September 30, 2013; date of final revised submission, February 12, 2014; date of acceptance, March 4, 2014.

Abbreviations Used

4-HNE = 4-hydroxynonenal
Ad = adenovirus
AMPK = AMP-activated protein kinase
BSA = bovine serum albumin
ChIP = chromatin immunoprecipitation
CS = cholesterol sulfate
DCF = 2′,7′-dichlorodihydrofluorescein
EGCG = epigallocatechin gallate
FBS = fetal bovine serum
GFP = green fluorescence protein
GOT = glutamic oxaloacetate transaminase
GPT = glutamic pyruvic transaminase
GPx1 = glutathione peroxidase 1
GSH = glutathione
GST = glutathione *S*-transferase
H_2DCFDA = H_2DCF-diacetate
H_2O_2 = hydrogen peroxide
H&E = hematoxylin and eosin
IL = interleukin
LPS = lipopolysaccharide
LXRα = liver X receptor α
MCD = methionine-choline deficient
MCS = methionine-choline sufficient
MDA = malondialdehyde
NASH = nonalcoholic steatohepatitis
NF-κB = nuclear factor-kappa B
OA = oleic acid
PAS-D = periodic acid-Schiff with diastase
PBS = phosphate-buffered saline
PPAR = peroxisome proliferator-activated receptor
qRT-PCR = quantitative real-time polymerase chain reaction
RORα = retinoic acid-related orphan receptor α
ROREs = ROR response elements
ROS = reactive oxygen species
SD = Sprague Dawley
si-RNA = small interference RNA
SOD2 = superoxide dismutase 2
SPR = surface plasmon resonance
TGFβ = transforming growth factor β
TNFα = tumor necrosis factor α